

Cylindrical Surfaces Enable Wavelength-Selective Extinction and Sub-0.2 nm Linewidth in 250 μm -Gap Silicon Fabry–Pérot Cavities

Maurine Malak, *Student Member, IEEE*, Frédéric Marty, Nicolas Pavy, Yves-Alain Peter, *Senior Member, IEEE*, Ai-Qun Liu, *Member, IEEE*, and Tarik Bourouina, *Senior Member, IEEE*

Abstract—In this paper, we propose two different designs of micromachined Fabry–Pérot optical cavities, with first motivation of improving the quality factor (Q -factor) and in the same time allowing increased cavity length L . Our approach consists of providing a solution to the main loss mechanism in conventional FP cavities related to the expansion of the Gaussian light beam after multiple reflections inside the cavity. The first design is based on all-silicon cylindrical Bragg mirrors, which provide 1-D confinement of light. In addition to wavelength selectivity, the first design also demonstrates its potential for a new class of applications, including wavelength selective extinction through mode-selective excitation, where the fiber-to-cavity distance is used as the control parameter. The second design is based on cylindrical Bragg mirrors combined with a fiber rod lens to provide a complete solution for 2-D confinement of light. This approach outperforms the first design in terms of Q -factor, of nearly 9000 for around 250 μm -long cavity, which suggests its potential use for biochemical sensing and analysis as well as cavity enhancement applications requiring high $Q \cdot L$ values. [2011-0162]

Index Terms—Curved Fabry–Pérot cavity, cylindrical bragg reflector, fiber rod lens (FRL), high Q -factor, mode-selective filter, wavelength selective extinction.

I. INTRODUCTION

OPTICAL FIBER communication is certainly the application area which led to the intensive research effort on optical microelectromechanical systems (MEMS) [1] including micro-optical resonators. Among these, silicon-based Fabry–Pérot (FP) cavities intended to wavelength division multiplexing have been developed as tunable filters [2]–[5] and

external cavity lasers [6], [7]. Such FP cavities also found interest in sensing application, including refractometry [8], [9], inertial sensing [10], gas sensing [11] and chemical and biological analysis [8], [12]. In most of these applications, the spectral line width is of special interest when considering the system performance, which is also related to the cavity finesse and quality factor (Q -factor). High Q -factors are desired to provide high distinction between specific wavelengths. Mirror reflectance is therefore of primary importance, and Bragg reflectors are preferred. These can result either from thin-film coatings [2]–[4], [13] or from silicon micromachining leading to silicon-air Bragg mirrors [5], [7], [14]–[16].

The early versions of FP cavities comprised two *planar* mirrors separated by the cavity gap length L . Due to its Gaussian nature, light undergoes many round trips between the mirrors while expanding before eventually getting out of the micromirrors boundaries by diffraction, due to their short heights, limited to a few tens of micrometers. That is why the planar resonators are referred to as unstable resonators [17]. This effect is responsible of the reduced quality factor observed in planar micromirrors, and it forces the designer to reduce the cavity length to few tens of micrometers to avoid excessive losses. Earliest reports about FP cavities based on spherical mirrors [17] demonstrate their excellent focusing capability. The curvature of the mirror focuses the beam in both transverse directions. Unlike FP cavities with planar mirrors, such resonators are considered as stable resonators because they prevent the light escape from the cavity boundaries. They were generally implemented from metallic gold-plated spherical mirrors to maintain a high reflectance and hence, a spectral response with high finesse.

In this paper, we propose a novel FP core architecture with two designs to overcome the limitations of planar FP cavities. The first design is inspired from the spherical resonators where we develop similar architecture but using curved mirrors of cylindrical shape [18]. Thus, we go one step forward over the planar resonators by curving the mirrors along one transverse plane to provide stability. Furthermore, in the second design, we combine the cylindrical mirrors together with a fiber rod lens (FRL) inside the cavity [19], to focus the beam in both transverse planes. This way, we emulate the spherical resonators using two discrete elements: The same curved cylindrical mirror, as in the first design, and the FRL, curved in the other transverse plane, which helps reducing the cavity losses and improves the Q -factor.

Manuscript received May 26, 2011; revised September 2, 2011; accepted October 6, 2011. Date of publication December 2, 2011; date of current version February 3, 2012. This work was supported in part by the French Embassy at Cairo (EGIDE Grant) and in part by ESIEE Paris. This work was presented in part at the IEEE MEMS 2011 Conference, Cancun, Mexico, January 23–27, 2011, and at the IEEE TRANSDUCERS Conference, Beijing, China, June 5–9, 2011. Subject Editor H. Zappe.

M. Malak, F. Marty, N. Pavy, and T. Bourouina are with the ESYCOM-Lab, ESIEE, Université Paris-Est, 93162 Noisy-le-Grand, France (e-mail: malakkam@esiee.fr; f.marty@esiee.fr; n.pavy@esiee.fr; t.bourouina@esiee.fr).

Y.-A. Peter is with the Department of Engineering Physics, Ecole Polytechnique de Montréal, Montréal, QC H3C 3A7, Canada (e-mail: yves-alain.peter@polymtl.ca).

A.-Q. Liu is with the School of Electrical and Electronic Engineering, Nanyang Technological University, Singapore 639798 (e-mail: eaqliu@ntu.edu.sg).

Color versions of one or more of the figures in this paper are available online at <http://ieeexplore.ieee.org>.

Digital Object Identifier 10.1109/JMEMS.2011.2174427

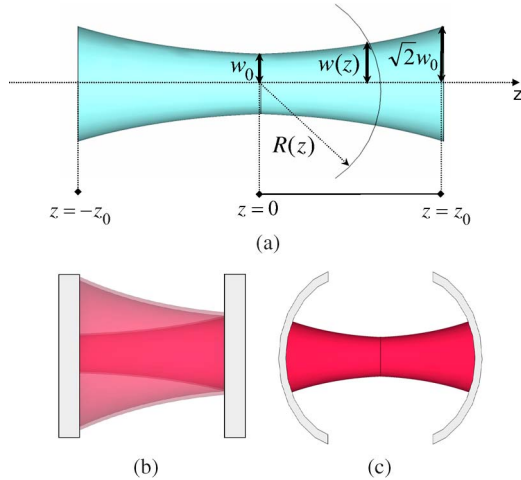


Fig. 1. Illustration of Gaussian beams properties. (a) Main geometrical characteristics. (b) Expansion of the spot size after multiple reflections by planar mirrors. (c) Confinement of the beam after multiple reflections by curved mirrors, whose radii of curvature fits with the beam radius of curvature at the specific mirror locations.

II. LIGHT CONFINEMENT BY CURVED REFLECTORS

As discussed earlier, conventional *in-plane* FP silicon microcavities, based on planar mirrors, were extensively studied [5], [7], [14]–[16], but such cavities are known to be unstable due to unavoidable losses. In fact, when considering a Gaussian beam, whose main characteristics are shown in Fig. 1(a) and which is typical of a light beam launched from a (lensed) optical fiber into the cavity, the beam spot size continuously expands after each round trip and eventually escapes the resonator boundaries [Fig. 1(b)]. This issue forces the designers to limit the cavity length to only a few tens of micrometers, as larger length implies higher losses, leading to rather poor performance. A rough evaluation of those limits of cavity dimensions is obtained by considering a Gaussian beam of waist w_0 launched in a cavity of length L and of lateral dimensions a . After propagating over a distance L , the beam radius $w(L)$ becomes

$$w(L) = w_0 \left[1 + \left(\frac{\lambda L}{\pi w_0^2} \right)^2 \right]^{\frac{1}{2}}. \quad (1)$$

The condition $w(L) < a/2$ must be satisfied before diffraction loss dominates. For small length L , when neglecting the corresponding term in (1), this condition reduces to $w_0 < a/2$. For larger L , the unity term can be neglected in (1) then, considering the upper limit $w_0 = a/2$, we finally obtain the condition: $a^2/\lambda L > 4/\pi$. Therefore, as also discussed in [17], the cavity Fresnel number $\mathfrak{N} = a^2/\lambda L$ must be larger than unity to allow the cavity supporting low loss.

Contrarily to cavities with planar mirrors, when considering curved mirrors whose radii of curvature fits the wavefront radius of curvature of the beam at specific locations, then light bounces back and forth without divergence [Fig. 1(c)], leading to the desired confinement.

Therefore, the concept idea consists first of replacing the planar mirrors by cylindrical Bragg mirrors that act like focusing lenses in the in-plane direction [Fig. 2(a)]. In the out-of-plane direction, the cavity behaves as an ordinary FP cavity

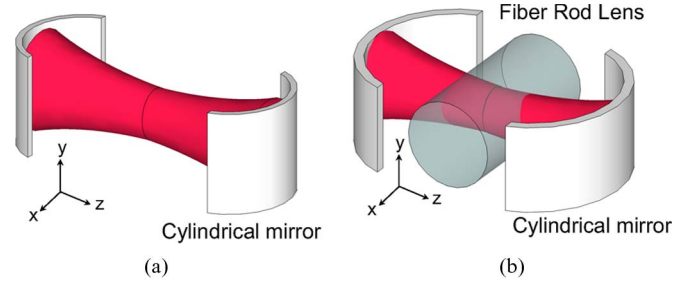


Fig. 2. Proposed designs of Fabry-Pérot microresonators with free-space propagation of light and confinement by curved surfaces. (a) Cylindrical mirrors insure in-plane 1-D confinement. (b) Additional FRL ensures out-of-plane confinement, leading to a complete solution for 2-D confinement and reduced optical loss.

with planar mirrors. In theory, an FP cavity with spherical mirrors (Curved in both in-plane and out-of-plane directions) would be the best choice for its focusing capability in both directions. In principle, such 3-D surfaces can be obtained by silicon micromachining [20]. However, when considering in-plane propagation of light, the technological challenge becomes much higher. That is why, based on the later FP principle and to overcome the technology limit, the authors have realized another type of stable FP cavity with a much higher performance than the first one as explained thereafter.

In this second design [Fig. 2(b)], we combine two major improvements: The first improvement takes advantage of the novel cylindrical Bragg mirrors that act as concave mirrors along one transverse direction, (in-plane). Hence, they focus the light beam, which is not the case when using planar mirrors. The second improvement concerns the FRL that has been introduced inside the cavity gap to focus the Gaussian beam in the other transverse direction (out-of-plane). This combination provides a complete focusing solution, leading to efficient light confinement inside the cavity.

III. DESIGN FOR 1-D LIGHT CONFINEMENT

The presented devices mainly consist of two cylindrical Bragg mirrors, whose radius of curvature is $R = 140 \mu\text{m}$, spaced apart by a distance $L = 210 \mu\text{m}$. The cylindrical mirror is made of an alternation of silicon and air layers. The silicon has a thickness of $3.67 \mu\text{m}$, while the air layer has a thickness of $3.49 \mu\text{m}$, both thicknesses correspond to an odd multiple of quarter the transmission wavelength (at $\lambda = 1550 \text{ nm}$) in silicon and in air, respectively. The device has been fabricated using the improved deep reactive ion etching (DRIE) process presented in [21]. SEM photo of the device is shown in Fig. 3(a).

In our first experiment, single mode fibers (SMF-28 from Corning) cleaved at 90° were used for recording the spectral response of different devices, which mainly differ in the number of Bragg layers per mirror, and this in turn, translates into different reflectance values. Fig. 4 shows the spectral responses obtained for three different cavities, corresponding to single, double, and triple silicon layer per mirror, respectively. Inspecting the results, the single layer cavity has a full width at half maximum (FWHM) = 3.11 nm , the double layer cavity has FWHM = 1.73 nm , and the three layers cavity has

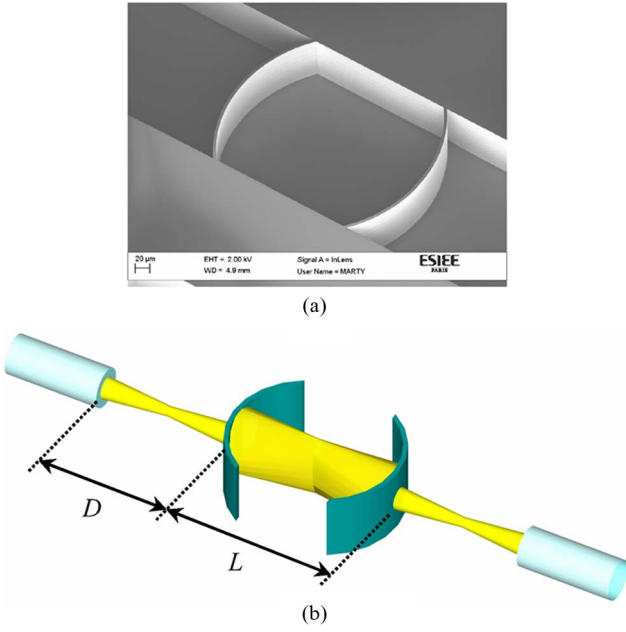


Fig. 3. FP resonator with cylindrical mirrors. (a) SEM photo of the fabricated device. (b) Schematic illustration of the (lensed) fiber positioning with respect to the cavity. The cavity length L governs wavelength tuning. The fiber-to-cavity distance D controls the selective excitation of transverse modes, leading to the behaviors of wavelength-selective extinction.

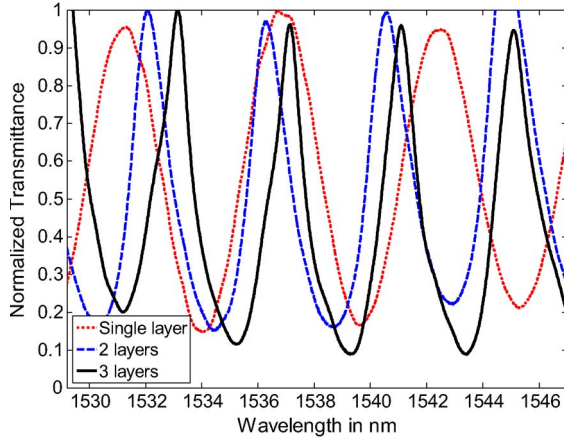


Fig. 4. Spectral response of FP cavities having one, two, and three silicon Bragg layers per mirror, respectively, revealing decreasing linewidths. The response of the single layer cavity is shifted with respect to the other responses due to the difference in the cavity effective length.

$\text{FWHM} = 1.42 \text{ nm}$. As expected, we conclude that as the number of silicon layer/mirror increases, the filter roll-off improves. It is noteworthy that the spectral responses of the three cavities are slightly shifted with respect to each other because their respective cavity effective lengths are slightly different due to the different thicknesses of the Bragg mirrors.

Analyzing the spectral responses, we deduced the values of the effective reflectance $\mathcal{R}_{\text{eff}} = T$, \mathcal{R} , which represents the product of the actual mirror reflectance \mathcal{R} and the intracavity transmittance T , with typically $T = e^{-\alpha 2L}$ to account for the distance-dependent intracavity loss. By calculating the finesse F from the previous data, and using

$$F = \frac{\text{FSR}}{\text{FWHM}} = \frac{\pi \sqrt{\mathcal{R}_{\text{eff}}}}{1 - \mathcal{R}_{\text{eff}}} \quad (2)$$

TABLE I
CHARACTERISTICS OF SINGLE, DOUBLE, AND THREE LAYERS CAVITIES AS DEDUCED FROM EXPERIMENTAL RESULTS

	FSR (nm)	FWHM (nm)	Finesse F	\mathcal{R}_{eff}	T_{Exp}	$\mathcal{R}_{\text{theory}}$
Single layer	5.79	3.11	1.862	21.59%	0.299	72%
Double layer	4.31	1.7273	2.495	30.48%	0.3133	97.3%
Three layers	3.935	1.4238	2.764	33.86%	0.3394	99.77%

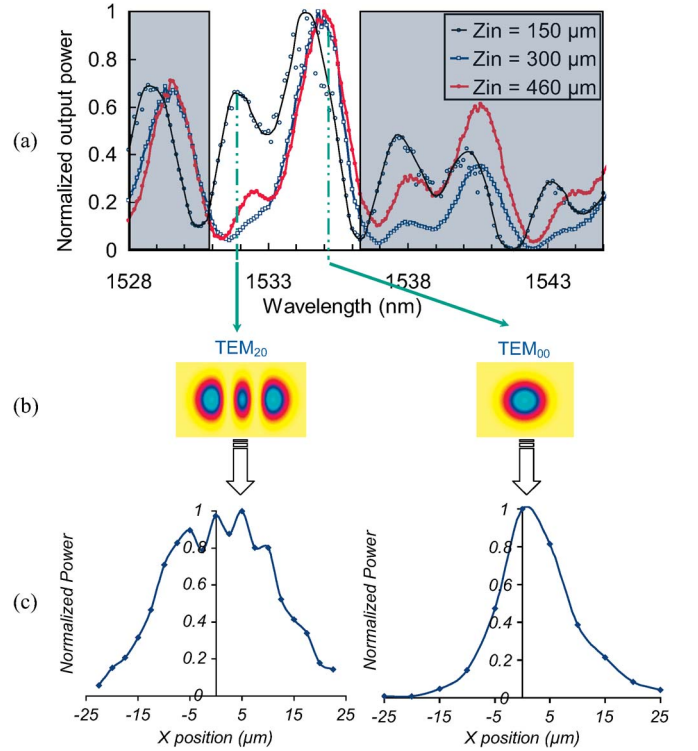


Fig. 5. Demonstration of wavelength selective extinction (and mode-selective filtering) of the FP cavity with cylindrical mirrors. (a) Recorded spectral responses of the cavity, measured with lensed fiber while varying the fiber-to-cavity distance D . The curves reveal selective excitation of the resonant transverse modes TEM_{20} around 1532 nm in addition to the fundamental Gaussian mode TEM_{00} . Varying D leads to different levels for mode TEM_{20} with an extinction ratio of 7 : 1. (b) Theoretical intensity distribution of TEM_{00} and TEM_{20} modes. (c) Measured intensity profiles (of modes TEM_{00} and TEM_{20}) obtained by lateral in-plane scanning of the detection fiber.

where FSR is the free spectral range of the cavity. Note that the use of the previous equation is a valid approximation as long as we are working in the limits of the paraxial approximation. Indeed, it helps getting a rough estimation of \mathcal{R}_{eff} . Moreover, from the knowledge of \mathcal{R}_{eff} and based on the theoretical values for \mathcal{R} , one can evaluate the intracavity transmittance T_{exp} of the measured structures. The corresponding results are given in Table I.

In a second experiment, a couple of lensed fibers having a spot size $2w_0 = 19 \mu\text{m}$ and a working distance $\text{WD} = 2z_0 = 300 \mu\text{m}$ were used for the characterization of the cavity with a single silicon layer. In this experiment, the excitation fiber was aligned at different input positions D , as shown in Fig. 3(b).

Wavelength sweep was carried out at three different D positions: $150 \mu\text{m}$, $300 \mu\text{m}$, and $460 \mu\text{m}$. The obtained responses

are shown in Fig. 5(a). We expected to find periodic response as in the first experiment. On the contrary, in addition to the periodic resonance peaks, some other resonance peaks arise.

To interpret the results of these experimental measurements, we have worked on the simulation and the modeling for the concerned structures. The modeling of the cavity (covered with more details in a separate publication) is developed in what follows, to interpret the additional peaks that appear in Fig. 5(a).

The cavity, case of study, is supposed to support Hermite–Gaussian transverse modes $\Psi_{m,n,q}$ [17], which are the typical modes of resonators made from spherical mirrors and whose analytical expression was adapted here to the cylindrical shape of the mirrors. In this case, the transverse degeneracy applies for order m only, along the x transverse direction (in-plane), while n is kept equal to 0 for the y direction (out-of-plane). Note that the fundamental modes ($m = 0, n = 0$)-with different values for q , are the longitudinal modes of the cavity, which are the only ones that can be supported by planar cavities. Therefore, for our cylindrical cavities, we will consider the following transverse modes:

$$\Psi_{m,0}(x, y) = \sqrt{\frac{\sqrt{2}}{w_x w_y}} H_m \left(\frac{\sqrt{2}x}{w_x} \right) e^{-\left(\frac{x^2}{w_x^2} + \frac{y^2}{w_y^2}\right)} e^{-jk \left(\frac{x^2}{2R_x} + \frac{y^2}{2R_y} \right)} \quad (3)$$

where $\Psi_{m,0}$ denotes the electric field transverse components representing the cavity electromagnetic resonant modes; w_x and w_y denote the beam size in the x and the y directions; R_x and R_y are the beam radii of curvature in the x and y directions; and H_m is the Hermite polynomial function of order m . As we are working in the limits of the paraxial approximation, we adopted the scalar notation for $\Psi_{m,0}$ for the TEM $_{m,0}$ modes as there is no longitudinal component of the electric field. Indeed, this is an acceptable approximation as the divergence angle of the studied Gaussian beam is less than 3.5° in our case and thus longitudinal components of the electric field can be neglected [17].

In addition, as we consider only the modes at the cavity entrance $z = 0$, then, the longitudinal (z) dependence of the cavity modes and the corresponding third mode order q do not appear in (3). There is a different set of transverse modes $\Psi_{m,0}$ for each longitudinal mode of order q . That is why the resonance spectrum in Fig. 5(a) is somehow periodic. Indeed, all the aforementioned modes have their own resonance frequencies, written as follows:

$$\nu_{m,n,q} = \frac{c}{2n_{\text{air}}L} \left[q + (1 + m + n) \frac{\arccos(1 - L/R)}{\pi} \right]. \quad (4)$$

$$\Gamma_{m,0} = \frac{\left| \int \int_{(D)} E_{\text{Fiber}}(x, y, 0) \cdot \Psi_{m,0}(x, y, 0) dx dy \right|^2}{\int \int_{(D)} |E_{\text{Fiber}}(x, y, 0)|^2 dx dy \cdot \int \int_{(D)} |\Psi_{m,0}(x, y, 0)|^2 dx dy} \quad (5)$$

TABLE II
THEORETICAL AND EXPERIMENTAL RESONANCE WAVELENGTHS FOR THE DIFFERENT (m, n, q) CAVITY MODES IN THE WAVELENGTH RANGE BETWEEN 1528 nm AND 1545 nm. THE WAVELENGTH VALUES OBSERVED EXPERIMENTALLY ARE GIVEN IN ITALIC CHARACTERS. EMPTY BOXES CORRESPOND TO MODES OUTSIDE THE CONSIDERED WAVELENGTH RANGE

Transverse mode orders (m,n)	Longitudinal mode order q	q=270	q=271	q=272	q=273	q=274
(0,0)	Theory			1540.5	1534.9	1529.3
	Experiment			<i>1540,6</i>	<i>1535</i>	<i>1529,5</i>
(2,0)	Theory	1544.7	1539.0	1533.4	1527,8	
	Experiment	<i>1543,9</i>	<i>1538,0</i>	<i>1532,4</i>	<i><1528</i>	
(4,0)	Theory	1537.5	1531.9			
	Experiment	<i>Not seen</i>	<i>Not seen</i>			

The corresponding resonance wavelengths are $\lambda_{m,n,q} = c/\nu_{m,n,q}$ where c is the speed of light in free space.

From the calculations of the resonant wavelengths using (4), we concluded that the additional peaks which appear in Fig. 5(a) pertain to the excitation of the transverse modes (TEM $_{20}$), while the higher order modes (TEM $_{40}$ and up) are not excited. It is worth mentioning that for symmetry reasons, and as confirmed through calculations (as well as by measurements), the modes with odd values of m cannot be excited by a pure Gaussian beam. The selectively coupled mode shapes of modes TEM $_{20}$ are graphed along with modes TEM $_{00}$ in Fig. 5(b).

The modes TEM $_{00}$ and TEM $_{20}$ were identified by calculating the resonance wavelengths of the different transverse modes inside the cavity. Table II shows a comparison between the experimental values of the resonant peak wavelengths of Fig. 5(a) and the theoretical values of the resonant wavelengths given by (4) where the mode order n was taken equal to 0. Data in Table II show the resonant wavelengths in the wavelength range of interest, which extends roughly between 1528 nm and 1545 nm corresponding to the wavelength range applied in our experiments. The cavity parameters are: $L = 210 \mu\text{m}$ and $R = 140 \mu\text{m}$. Among all resonance modes that can theoretically be excited (even numbers for m), only modes (0,0) and (2,0) are found experimentally as indicated in Table II. This is ascribed to the different efficiencies in mode matching with the injected pure Gaussian beam, as discussed hereafter.

Next is the model concerning the fiber-to-cavity power coupling efficiency $\Gamma_{m,0}$ of the fiber Gaussian beam into the cavity TEM $_{m,0}$ modes. Calculations are done numerically based on overlap integral in (5), shown at the bottom of the page, where

TABLE III
THEORETICAL AND EXPERIMENTAL POWER COUPLING
EFFICIENCIES CALCULATED USING (5) FOR MODES
TEM_{0,0} UP TO TEM_{4,0}. FOR $D = 460 \mu\text{m}$

	$\Gamma_{0,0}$	$\Gamma_{1,0}$	$\Gamma_{2,0}$	$\Gamma_{3,0}$	$\Gamma_{4,0}$
Theory	89,14 %	0 %	9,15 %	0 %	1,41 %
Experiment	89 %	0 %	11 %	0 %	0 %

E_{Fiber} is the transverse component of the electric field injected from the lensed fiber, considered as a pure Gaussian beam

$$E_{\text{Fiber}}(x,y,z=0) = E_0 \sqrt{\frac{\sqrt{2}}{w_x w_y}} e^{-\left(\frac{x^2}{w_x^2} + \frac{y^2}{w_y^2}\right)} e^{-jk\left(\frac{x^2}{2R_x} + \frac{y^2}{2R_y}\right)}. \quad (6)$$

The calculation domain (D) extends from $-100 \mu\text{m}$ to $100 \mu\text{m}$ in both X and Y directions; the Bragg mirror is assumed to be thin and transparent in the infrared range. Thus, the injected field crosses the cavity, keeping the initial values of the beam size and radii of curvature.

Calculations of the coupling efficiencies $\Gamma_{m,0}$ defined in (5) were performed in the case of the coupling distance $D = 460 \mu\text{m}$, for values of m ranging from 0 to 4. The corresponding results are presented in Table III, along with the experimental values of $\Gamma_{m,0}$ extracted from the data of Fig. 5(a). The calculation results reveal a significant coupling to transverse modes (0,0) and (2,0), as well as a drastic decrease, down to 1.4%, for coupling to mode (4,0), which was not observed experimentally. The calculated coupling efficiency vanishes for odd values of m , which is consistent with the fact that the corresponding resonant wavelengths were not observed experimentally. For all modes, Table III also reveals a very good quantitative agreement between calculated and experimental values.

For further discussion, one can also mention that in general, the fact that a cavity is able to support or not the higher order modes strongly depends on its dimensions. In addition to cavity length L , here the role of mirror radius of curvature R is very important and is usually taken into account in the models found in the literature through the so-called g -factor $g = 1 - L/R$. While cavities with parallel mirrors ($g = 1$) can support only longitudinal modes (the fundamental modes TEM_{0,0}), the resonators with curved mirrors are able, in principle, to support higher order (transverse) modes. However, those modes will appear or not, depending on the corresponding round-trip loss inside the cavity, which also depends on the cavity Fresnel number $\aleph = a^2/\lambda L$ introduced above. This subject was studied in detail since the early 1960s in the case of spherical mirrors, namely by Boyd and Gordon [22] and by Fox and Li [23], who took into account the diffraction effects on the mirrors. In our work, we have $\aleph = 15$ and two different values for the g -factor, $g_y = -0,5$ and $g_x = 1$, due to the cylindrical shape of our mirrors. According to the model developed in [23], both values of g_x and g_y and the rather large value of \aleph of our cavities lead to excellent stability conditions. This applies at least for the lowest mode orders, the trend being that a gradual degradation of stability is observed as the mode orders increase [22], which is consistent with the experimental fact

that the best coupled modes in our case are, by order, mode TEM_{0,0} and then mode TEM_{2,0}. However, according to the good theory/experience agreement found in Table III for the coupling efficiencies, one may conclude that in our case, the limitation on the considered transverse modes is due to coupling conditions, not to the diffraction effects.

Looking over the experimental results in Fig. 5(a), we come out with the following potential applications of this device.

- 1) The first observation suggests that the device behaves as a *mode-selective filter*. In this case, the device can be used for the purpose of selecting only longitudinal modes (TEM_{0,0}) and reject the transverse modes (TEM_{2,0} and higher order modes). In the context of such application, the user will keep the distance D constant at $300 \mu\text{m}$, leading to the transmission of (TEM_{0,0}) modes only, whatever was their wavelength.
- 2) On the contrary, if the concern is about the distribution of light intensity inside the cavity; then switching from mode (TEM_{0,0}) to mode (TEM_{2,0}) can be exploited. In the context of such practical application, the user will keep the distance D constant at $150 \mu\text{m}$, then, switch the excitation λ from 1535 nm (TEM_{0,0}) to 1532 nm (TEM_{2,0}).
- 3) The third application would be *Wavelength selective switching*. In this case, we keep the excitation λ at 1532 nm corresponding to the (TEM_{2,0}) transverse mode. Controlling the distance D (the fiber-to-cavity distance) also denoted z_{in} in Fig. 5(a), we can bring the mode TEM_{2,0} (at 1532 nm) from ON to OFF states and vice versa, while the mode TEM_{0,0} (at 1535 nm) is unaffected and stays always in the ON state. The extinction ratio, defined as the ratio between the highest and the lowest power levels is $7 : 1$. In addition to the previously reported MEMS-based wavelength-selective switching solution [24], our device can potentially lead to an alternative MEMS-compatible wavelength-selective switching technique, in which the control of the distance D can be implemented for instance by adding a movable mirror, whose motion acts on the optical path from the fixed fiber to the fixed cavity.
- 4) The latter behavior also suggests another application, which consists of an *Add-Drop multiplexer*. In such application, we inject the wavelengths of 1532 nm and 1535 nm , corresponding to different communication channels; then by switching D from $150 \mu\text{m}$ to $300 \mu\text{m}$, the channel at $\lambda = 1532 \text{ nm}$ is either added or dropped to the readily existing channel at $\lambda = 1535 \text{ nm}$.

It is worth mentioning that the device in its actual form still lacks in performance for those practical applications. In particular, the insertion loss (which does not appear in the normalized plots shown in Fig. 5) is too high, in the order of 28 dB , while the contrast (ratio of maximum transmitted power to minimum transmitted power) is in the order 13 dB . Various directions can be followed to reduce the insertion loss. We can classify them into design aspects and technological aspects. One design aspect suggests the reduction of the radius of curvature as confirmed by our experimental results. The

technological aspects suggest further smoothing for the *external* sidewalls of the Bragg mirrors, which do not benefit from the same smoothness as in the *inner* thin trenches of the Bragg mirrors, as discussed at the end of Section IV. The fabricated dies have not yet been subjected to any post DRIE treatment for sidewall smoothing, which we believe lying behind the relatively high insertion loss. Another technology direction suggests using etching at cryogenic temperatures to get a better quality for the Bragg mirrors [25].

IV. DESIGN FOR 2-D LIGHT CONFINEMENT

A. Quality Factor: Experiment and Analysis

As mentioned above, the design schematically shown in Fig. 2(b) provides a complete solution for 2-D confinement of light, due to the additional cylindrical surface of the FRL inserted inside the cylindrical silicon cavity. Such devices were designed, realized, and measured. All fabricated devices share common parameters. Every silicon layer has a width of $3.67 \mu\text{m}$, while the air layer has a width of $3.49 \mu\text{m}$. A long recess opening ($\sim 1 \text{ cm}$) of $128 \mu\text{m}$ width is shared between all the devices to facilitate the insertion of the FRL, whose width is $125 \mu\text{m}$. On the contrary, the fabricated FP cavities differ from each other, either in their physical length of the cavity or in the number of Bragg layers per mirror. Based on these settings, many combinations were generated, measured, and then analyzed. Photographs of a fabricated device are shown in Fig. 6.

The fabricated devices were measured using in-plane injection and detection by cleaved fibers. A tunable laser source is used in conjunction with a power meter for achieving the wavelength sweep and recording the spectral response. The minimum recorded full width at half maximum (FWHM) is 0.1765 nm leading to a Q -factor of 8818. These values are obtained for the cavity *A* having four silicon-air layers per mirror and a physical length $L = 265.8 \mu\text{m}$ and $R = 140 \mu\text{m}$. Fig. 7 shows the measured spectral response of this device. It is noteworthy, in our case, that the physical length is different from the optical length due to the presence of the FRL whose refractive index $n = 1.47$. Thus, the optical length is equal to $324.6 \mu\text{m}$.

Other devices with different number of Bragg layers were tested to study the impact of the mirror reflectance on the Q -factor. The corresponding results are shown in Fig. 8. We find that as the number of layers N increases, the Q -factor increases accordingly up to $N = 4$ where $Q = 8818$. The results obtained confirm the trend of the Q -factor observed in an ideal FP cavity with planar mirrors and given by

$$Q = \frac{2\pi nL}{\lambda_0} \left(\frac{\sqrt{\mathfrak{R}_{\text{eff}}}}{1 - \mathfrak{R}_{\text{eff}}} \right) \quad (7)$$

with $\mathfrak{R}_{\text{eff}} = \Gamma \cdot \mathfrak{R}$.

The previous rule breaks as N increases further, since the Q -factor diminishes to $Q = 6068$ for $N = 5$. This might be attributed to the tolerance on the critical dimension (defined as the ideal thickness of the Bragg layers, to fulfill the requirement of odd multiple of quarter wavelength), which becomes

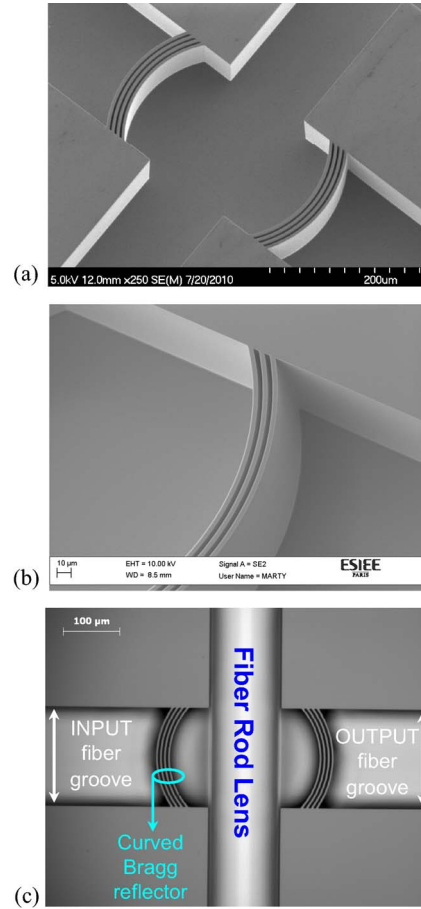


Fig. 6. Fabricated resonator for 2-D confinement of light (a) SEM photos of FP cavity with Bragg mirrors of cylindrical shape (here four silicon-air layers with the wide DRIE trench for the FRL). (b) SEM photo showing a closer view on a Bragg mirror (here three silicon-air layers). (c) Microscopic photo of the silicon structure including the FRL placed inside the DRIE recess for the purpose of “vertical” out-of-plane collimation.

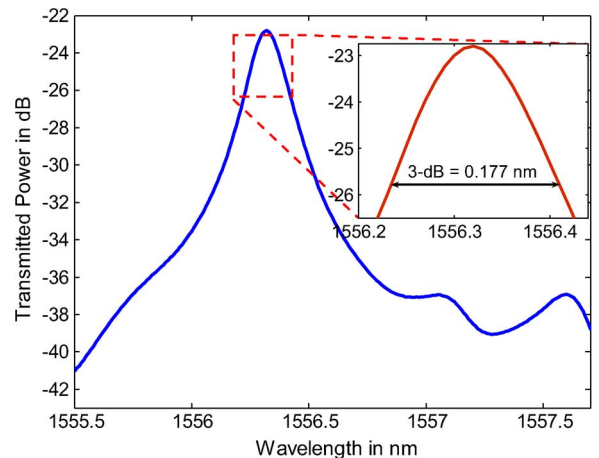
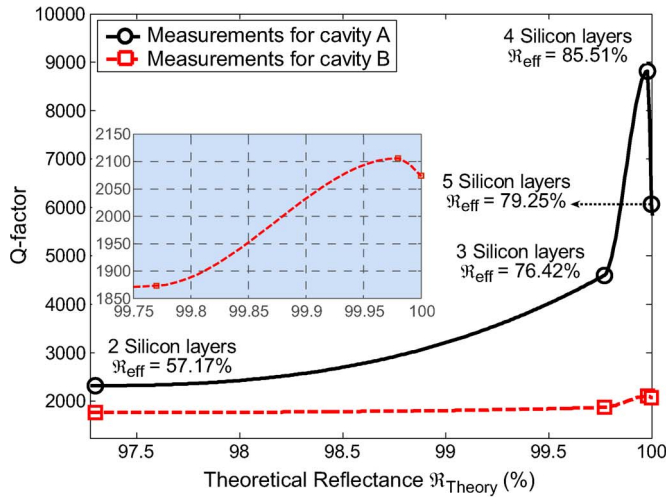
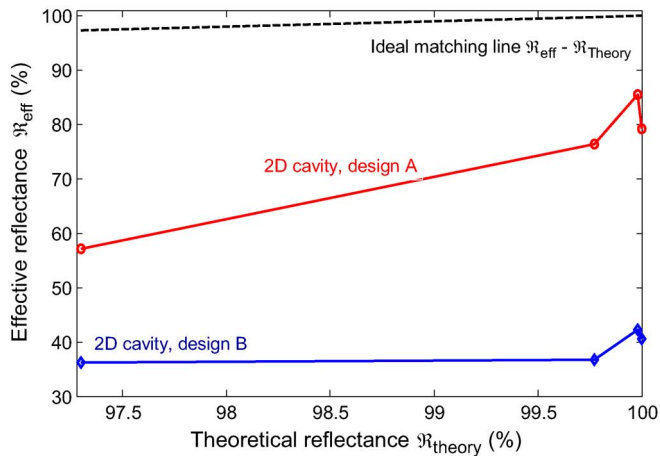


Fig. 7. Measured spectral response on a cavity of length $L = 265.8 \mu\text{m}$. Designed with cylindrical mirrors of radius of curvature $R = 140 \mu\text{m}$ with four silicon-air Bragg layers. The linewidth is 0.177 nm also corresponding to a Q -factor of 8818.

more pronounced as N increases. The tolerance on the critical dimension reduces \mathfrak{R} below the theoretically estimated values $\mathfrak{R}_{\text{Theory}}$, which in turn degrades Q . A similar trend was observed for cavity *B* with $R = 200 \mu\text{m}$. The inset in Fig. 8(a)



(a)



(b)

Fig. 8. (a) Experimental values of Q -factor versus theoretical reflectance of the curved Bragg mirrors for the two cavities A and B : Cavity A has a length $L = 265.8 \mu\text{m}$ and radius of curvature $R = 140 \mu\text{m}$. Cavity B has $L = 385.6 \mu\text{m}$ and $R = 200 \mu\text{m}$. The inset is a zoom of the design B illustrating the degradation in the Q -factor as observed for cavity A . (b) Effective reflectance $\mathfrak{R}_{\text{eff}}$ versus theoretical reflectance $\mathfrak{R}_{\text{Theory}}$ for the two cavities A and B of the 2-D design. The comparison is also given with respect to the ideal case.

shows a magnified view of the experimental results for cavity B having $R = 200 \mu\text{m}$ illustrating a similar degradation in the Q -factor as observed for the cavity A with $R = 140 \mu\text{m}$. It is worth to mention that the latter cavity was found to perform better since the cavities with larger R tend to the behavior of the cavities based on planar reflectors.

Using (2), as in the previous section, for estimating $\mathfrak{R}_{\text{eff}}$ from the experimental result shown in Fig. 8, we found that for an $\text{FSR} = 3.5 \text{ nm}$ and $\text{FWHM} = 0.1765 \text{ nm}$, $\mathfrak{R}_{\text{eff}} = 85.51\%$ compared to $\mathfrak{R}_{\text{Theory}} = 99.98\%$. The discrepancy between both values is due to many reasons. Among these, we can cite: 1) the tolerance on the critical dimension, which is introduced by overetching of the Bragg layers and reduces the reflectance below the expected value; 2) the mirrors surfaces which are not perfectly vertical; 3) these surfaces are not perfectly smooth, as they exhibit some roughness which induces scattering losses; 4) the reflections at the interfaces of the FRL decrease the intracavity transmittance T , which is supposed to be higher than

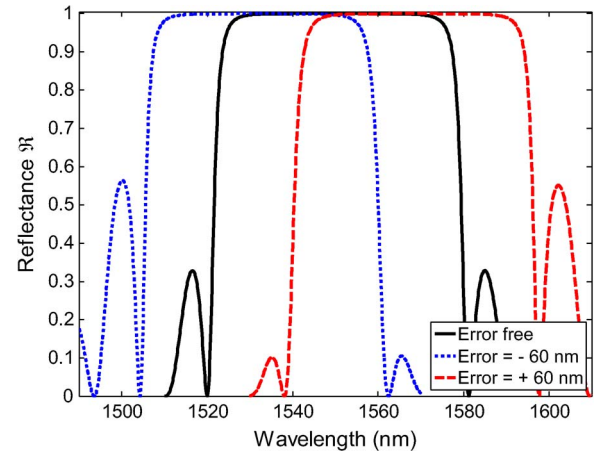


Fig. 9. Simulated reflectances of the multilayered Bragg mirrors with an introduced error $\pm 60 \text{ nm}$ to study the impact of the technological error on the device performance. The error-free response is also shown in the graph, as a reference.

in the first design, but is still well below 100%. An attempt to evaluate the impact of these effects is discussed here below.

The loss on the critical dimension has been simulated by introducing a finite error ($\pm 60 \text{ nm}$) in the silicon layer thickness. The simulations are based on the developed model for multilayered stack theory [26] used for planar mirrors. We assume that the use of this model is valid in our case as we are in the limits of the paraxial approximation. The simulation results are shown in Fig. 9.

The introduced error ($\delta t \approx \pm 60 \text{ nm}$) shifts the overall reflectance bandwidth about ($\delta \lambda \approx \pm 20 \text{ nm}$). Hence, if the fabrication technologically introduces an error of $\delta t = -60 \text{ nm}$, and considering our operating point the wavelength $\lambda = 1556 \text{ nm}$, then instead of getting a reflectance $\mathfrak{R} = 99.98\%$ in the ideal design, we get $\mathfrak{R} = 96\%$.

DRIE ideally gives vertical profiles, but there is practically a slight deviation angle α from such ideal 90° angle. Our devices are made from silicon walls whose depth is $a = 77 \mu\text{m}$ and whose thickness is ideally $t = 3.67 \mu\text{m}$. This means that the minimum requirement to produce such walls is that α must be less than 1.4° . In our case, we manage with process optimization to achieve values of α which do not exceed 0.1° . In these conditions, the difference of wall thickness at the top and at the bottom of the Bragg walls is in the order of $2a \sin(\alpha) \approx 270 \text{ nm}$. Considering now that the light spot does not shine the whole wall depth but only a portion of it about $a^* = 20 \mu\text{m}$, then this difference reduces to nearly 70 nm , whose impact is in the same order of the effect discussed in the previous paragraph.

DRIE using the Bosch process is also known to produce fluorocarbon residues as well as scalloping in the form of quasiperiodic roughness. The former is removed by post-DRIE processing. As for the latter, it is known that scalloping usually leads to a surface roughness which can exceed 200 nm . Fortunately, when considering small trenches (in the range below $5 \mu\text{m}$) as those used in our Bragg mirrors, this roughness drastically reduces to levels below 25 nm and eventually vanishes, while the aspect ratio increases during the process, as detailed in a previous report [27]. Practically, this means that any residual roughness will be observable only at the top of the trenches and

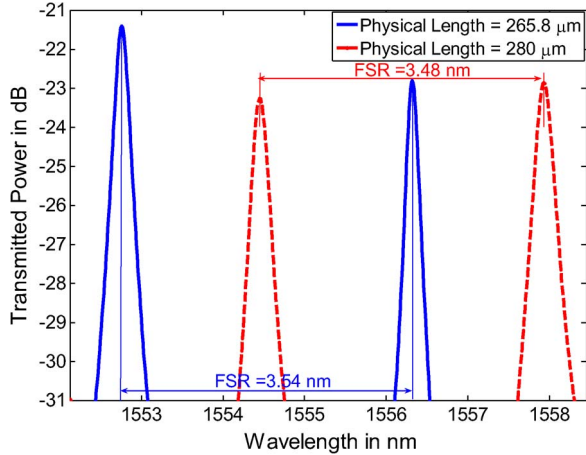


Fig. 10. Measured spectral response of FRL cavities with two different cavity lengths $L = 265.8$ and $280 \mu\text{m}$. (The cylindrical mirrors have four silicon-air layers).

disappears at a depth of nearly $25 \mu\text{m}$, corresponding for our trenches to the threshold aspect ratio of 7 highlighted in [27].

Regarding the loss introduced by reflections on the FRL, it can be taken into account simply by multiplying the initial intracavity transmittance T , by another transmittance term T^* to describe the air-glass-air transition of the light beam. Considering the fiber refractive index value $n_f = 1.47$ and neglecting possible multiple reflections inside the fiber, an estimate of such second transmittance term is in the order of $T^* = 4n_f/(1 + n_f)^2 \approx 0.96$.

To mimic the tunability behavior of our resonators, spectral measurements have been carried out for cavities having similar characteristics but differing only in their physical lengths. Two different cavity physical lengths ($L = 265.8$ and $280 \mu\text{m}$) have been measured, both are based on four silicon layers per mirror with a radius of curvature $R = 140 \mu\text{m}$. The spectral responses are superimposed in Fig. 10.

Furthermore, a simple test has been done to highlight the importance of the FRL on the cavity performance. In this test, a device based on two silicon-air layers per mirror has been measured with and then without the insertion of the FRL. Though the reflectance of the two silicon-air layers is not very high, this device has been chosen for this specific illustration because it obeys the stability conditions (as discussed in the next section) in both cases: with and without the FRL. The corresponding measurements results, shown in Fig. 11, reveal that the Q -factor improves by a factor of $3.68\times$ for resonance wavelength around 1615 nm , also revealing transverse modes. A similar improvement ($4\times$) of the Q -factor has also been recorded for a cavity based on mirrors with three silicon layers.

B. Design for Stability

The two cavities A and B studied above exhibit different behaviors in terms of stability; the first is stable, while the second is unstable. This fact can be confirmed by the following analytical calculations, which also give the guidelines for further designs of optical resonators ensuring a stable behavior.

For this purpose, and starting from the analytical model presented in [28], we develop new relations that link the cavity

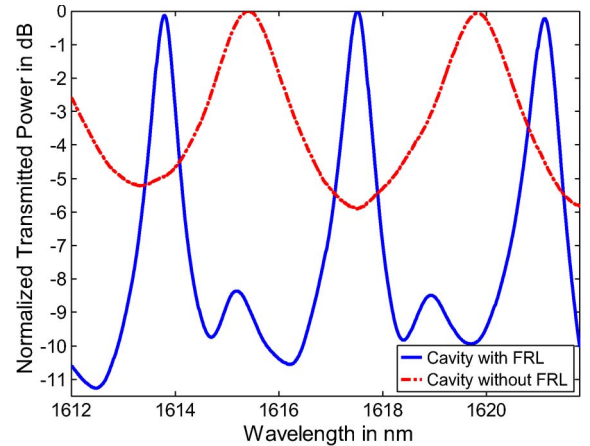


Fig. 11. Comparison of measured responses with and without the FRL, illustrating the ($3.68\times$) improvement in the Q -factor. (Here, the mirrors consist of two silicon-air layers).

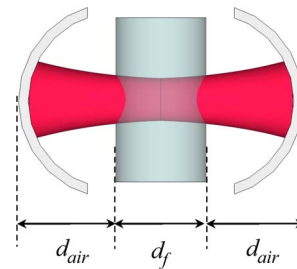


Fig. 12. Top view of the FRL resonator design seen in the XZ transverse plane, illustrating the distances of propagation inside the fiber d_f and in air: twice d_{air} .

radius of curvature to the free space propagation distance inside the FRL cavity as shown in Fig. 12, where the geometrical parameters used in our model are defined.

Considering the XZ cross section (top view as shown in Fig. 12), and for the YZ cross section (side view), respectively, the stability conditions are given by [28]

$$0 \leq \frac{(2d_{\text{air}} + d_f/n_f)}{2|R|} \leq 1 \quad (8a)$$

$$0 \leq (1 - 2/n_f) + (4d_{\text{air}}/d_f)(1 - 1/n_f) \leq 1. \quad (8b)$$

Hence, we get at the upper limits

$$\left(1 - \frac{2}{n_f}\right) + \left(\frac{4d_{\text{air}}}{d_f}\right) \left(1 - \frac{1}{n_f}\right) = 1 \quad (9a)$$

$$d_{\text{air}} = R - \frac{d_f}{2n_f}. \quad (9b)$$

From (9), we obtain at the end

$$d_{\text{air-max}} = \frac{d_f}{2(n_f - 1)} \quad (10a)$$

$$R_{\text{max}} = \frac{d_f}{2} \left\{ \frac{2n_f - 1}{n_f(n_f - 1)} \right\}. \quad (10b)$$

Similarly, one obtains for the lower limits

$$d_{\text{air-min}} = \frac{d_f}{4} \left\{ \frac{2 - n_f}{n_f - 1} \right\} \quad (11a)$$

TABLE IV

DESIGN PARAMETERS FOR REACHING THE STABILITY CONDITIONS FOR RESONATOR DESIGN INCLUDING THE FRL. THE STUDIED CAVITY *A* HAS A LENGTH $L = 265.8 \mu\text{m}$ AND RADIUS OF CURVATURE $R = 140 \mu\text{m}$ AND IS STABLE. THE STUDIED CAVITY *B* HAS $L = 385.6 \mu\text{m}$ AND $R = 200 \mu\text{m}$ AND IS UNSTABLE

	Ranges for stability	Studied devices	
		Cavity A	Cavity B
d_f (μm)	125 (fixed)	125	125
R (μm)	Range [77.8, 175.5]	140	200
d_{air} (μm)	Range [35.2, 133.0]	70.2	130.3
Stability	Yes, as long as conditions on R , d_{air} and d_f are satisfied simultaneously	Yes	No

$$R_{\min} = \frac{d_f}{4} \left\{ \frac{2}{n_f} + \frac{2 - n_f}{n_f - 1} \right\}. \quad (11b)$$

For the FRL cavities considered in this paper, knowing that $d_f = 125 \mu\text{m}$ and $n_f = 1.47$, one obtains the range of dimensions leading to a stable behavior, as summarized in Table IV. This table also includes the specific characteristics and stability behavior of cavities *A* and *B* that were studied experimentally.

V. CONCLUSION

In conclusion, two new designs of FP cavities based on curved surfaces have been presented. Our first motivation was to improve the performance as compared with the FP cavities based on planar mirrors. The first design based on cylindrical Bragg mirrors revealed preferential excitation of transverse modes TEM_{20} under certain conditions, governed by the fiber-to-cavity distance. This makes this design an interesting candidate for several applications in the MEMS domain, including wavelength selective switch. An analytical model was developed for this design. It was validated through quantitative comparison with experimental data; it helped understanding the behavior of the first resonator. It also provides a design tool for further optimization. The second design which combines both the cylindrical Bragg mirrors and a FRL shows a higher performance in terms of Q -factor. The maximum recorded value was $Q = 8818$ for a cavity built with Bragg reflectors having four silicon layers. The corresponding finesse F is 20; it remains much below the values that can be found in previous reports; for instance F exceeding 1000 as reported in [29]. In our case, both devices share the advantage of high Q -factor and long cavity length $L > 200 \mu\text{m}$, which can also be expressed in terms of a figure of merit $Q \cdot L$, which is up to $Q \cdot L = 2 \cdot 10^6 \mu\text{m}$ for the second design and which is convenient for cavity enhancement applications including chemical sensing.

Relations have been derived between the maximum (minimum) values of mirror radius of curvature R and the free space propagation distance d_{air} in air that maintain a stable behavior for the optical resonator of the 2-D design. For both designs, the measured data have been analyzed to deduce the effective reflectance of the curved mirrors. The impact of the technological error has been evaluated through simulations.

The best recorded linewidths on our two designs are 1.42 nm and 0.18 nm, respectively, for the first and the second resonator

designs, respectively. Regarding their potential use in DWDM systems and considering the International Telecommunication Union grid standards, the first design might be suitable for the 200 GHz channel-spacing grid, while the second design might be suitable for systems down to the 25 GHz channel spacing. Indeed, the former and the latter are also equivalent to nearly 1.6 nm and 0.2 nm, respectively, in terms of wavelength spacing requirements. Nevertheless, further improvement of our devices is needed to fit other DWDM requirements, In particular, the insertion loss measured on our devices is still too high, in the range of 20–30 dB.

REFERENCES

- [1] L. Y. Lin and E. L. Goldstein, "Opportunities and challenges for MEMS in lightwave communications," *IEEE J. Sel. Top. Quantum Electron.*, vol. 8, no. 1, pp. 163–172, Jan./Feb. 2002.
- [2] D. Sadot and E. Boimovich, "Tunable optical filters for dense WDM networks," *IEEE Commun. Mag.*, vol. 36, no. 12, pp. 50–55, Dec. 1998.
- [3] D. Hohlfeld, M. Epmeier, and H. Zappe, "A thermally tunable, silicon-based optical filter," *Sens. Actuators A, Phys.*, vol. 103, no. 1/2, pp. 93–99, Jan. 2003.
- [4] K. Yu and O. Solgaard, "Tunable optical transversal filters based on a Gires-Tournois interferometer with MEMS phase shifters," *IEEE J. Sel. Topics Quantum Electron.*, vol. 10, no. 3, pp. 588–597, May/Jun. 2004.
- [5] B. Saadany, M. Malak, M. Kubota, F. Marty, Y. Mita, D. Khalil, and T. Bourouina, "Free-space tunable and drop optical filters using vertical bragg mirrors on silicon," *IEEE J. Sel. Topics Quantum Electron.*, vol. 12, no. 6, pp. 1480–1488, Nov./Dec. 2006.
- [6] H. Cai, X. M. Zhang, A. B. Yu, Q. X. Zhang, and A. Q. Liu, "MEMS tuning mechanism for eliminating mode hopping problem in external-cavity lasers," in *Proc. 20th IEEE Int. Conf. Micro Electro Mech. Syst.*, 2007, pp. 159–162.
- [7] J. Masson, R. St-Gelais, A. Poulin, and Y.-A. Peter, "Tunable fiber laser using a MEMS-based in-plane Fabry–Pérot filter," *J. Quantum Electron.*, vol. 46, no. 9, pp. 1313–1319, Sep. 2010.
- [8] W. Z. Song, X. M. Zhang, A. Q. Liu, C. S. Lim, P. H. Yap, and H. M. M. Hosseini, "Refractive index measurement of single living cells using on-chip Fabry–Pérot cavity," *Appl. Phys. Lett.*, vol. 89, no. 20, pp. 203901-1–203901-3, Nov. 2006.
- [9] R. St-Gelais, J. Masson, and Y.-A. Peter, "All-silicon integrated Fabry–Pérot cavity for volume refractive index measurement in microfluidic systems," *Appl. Phys. Lett.*, vol. 94, no. 24, pp. 243905-1–243905-3, Jun. 2009.
- [10] K. Zandi, B. Wong, J. Zou, R. V. Kruzelecky, W. Jamroz, and Y.-A. Peter, "In-plane silicon-on-insulator optical MEMS accelerometer using waveguide Fabry–Pérot microcavity with silicon/air bragg mirrors," in *Proc. 23rd IEEE Int. Conf. Micro Electro Mech. Syst.*, 2010, pp. 839–842.
- [11] G. Lammel, S. Schweizer, and P. Renaud, "MEMS infrared gas spectrometer based on a porous silicon tunable filter," in *Proc. 14th IEEE Int. Conf. Micro Electro Mech. Syst.*, 2001, pp. 578–581.
- [12] H. Shao, D. Kumar, and K. L. Lear, "Single-cell detection using optofluidic intracavity spectroscopy," *IEEE Sensors J.*, vol. 6, no. 6, pp. 1543–1550, Dec. 2006.
- [13] W. Liu and J. J. Talghader, "Spatial-mode analysis of micromachined optical cavities using electrothermal mirror actuation," *J. Microelectromech. Syst.*, vol. 15, no. 4, pp. 777–785, Aug. 2006.
- [14] S. Yun and J. Lee, "A micromachined in-plane tunable optical filter using the thermo-optic effect of crystalline silicon," *J. Micromech. Microeng.*, vol. 13, no. 5, pp. 721–725, Sep. 2003.
- [15] M. W. Pruessner, T. H. Stievater, and W. S. Rabinovich, "Reconfigurable filters using MEMS resonators and integrated optical microcavities," in *Proc. IEEE MEMS Conf.*, 2008, pp. 766–769.
- [16] A. Lipson and E. M. Yeatman, "A 1-D photonic band gap tunable optical filter in (110) silicon," *J. Microelectromech. Syst.*, vol. 16, no. 3, pp. 521–527, Jun. 2007.
- [17] A. Yariv, *Quantum Electronics*, 3rd ed. Hoboken, NJ: Wiley, 1989.
- [18] M. Malak, N. Pavy, F. Marty, and T. Bourouina, "Mode-selective optical filtering and wavelength-selective switching through Fabry–Pérot cavity with cylindrical reflectors," in *Proc. 16th Int. Conf. Solid-State Sens., Actuators Microsyst., Transducers*, Beijing, China, 2011, pp. 534–537.

- [19] M. Malak, N. Pavy, F. Marty, Y.-A. Peter, A. Q. Liu, and T. Bourouina, "Stable, high-Q Fabry-Perot resonators with long cavity based on curved, all-silicon, high reflectance mirrors," in *Proc. 24th IEEE Int. Conf. Micro Electro Mech. Syst.*, 2011, pp. 720–723.
- [20] T. Bourouina, T. Masuzawa, and H. Fujita, "The MEMSNAS process: Microlensing effect for micromachining 3D structures of nearly all shapes," *J. Microelectromech. Syst.*, vol. 13, no. 2, pp. 190–199, Apr. 2004.
- [21] F. Marty, L. Rousseau, B. Saadany, B. Mercier, O. Français, Y. Mita, and T. Bourouina, "Advanced etching of silicon based on deep reactive ion etching for silicon high aspect ratio microstructures and three-dimensional micro and NanoStructures," *Microelectron. J.*, vol. 36, no. 7, pp. 673–677, Jul. 2005.
- [22] G. D. Boyd and J. P. Gordon, "Confocal multimode resonator for millimeter through optical wavelength masers," *Bell Syst. Tech. J.*, vol. 40, pp. 489–508, 1961.
- [23] A. G. Fox and T. Li, "Modes in a maser interferometer with curved and tilted mirrors," *Proc. IEEE*, vol. 51, no. 1, pp. 80–89, Jan. 1963.
- [24] K. Yu, N. Park, D. Lee, and O. Solgaard, "A wavelength selective switch with flat passband using a free-space grating and MEMS phase-shifters," in *Proc. QELS Conf.*, Baltimore, MD, May 22, 2005, vol. 2, pp. 978–980.
- [25] B. Saadany, D. Khalil, and T. Bourouina, "Highly efficient micromachined bragg mirrors using advanced DRIE process," in *Proc. IEEE Int. Conf. MEMS, NANO Smart Syst.*, Cairo, Egypt, Dec. 2006, pp. 48–51.
- [26] H. A. Macleod, *Thin Film Optical Filters*. London, U.K.: Inst. Phys. Publ., 2001.
- [27] Y. Mita, M. Kubota, M. Sugiyama, F. Marty, T. Bourouina, and T. Shibata, "Aspect ratio dependent scalloping attenuation in DRIE and an application to low-loss fiber-optical switch," in *Proc. IEEE MEMS Conf.*, Istanbul, Turkey, Jan. 22–26, 2006, pp. 114–117.
- [28] M. Malak, T. Bourouina, N. Pavy, E. Richalot, F. Marty, and A.-Q. Liu, "Design, modeling and characterization of stable, high Q-factor curved Fabry-Pérot cavities," *J. Microsyst. Technol.*, vol. 17, no. 4, pp. 543–552, Apr. 2011.
- [29] R. S. Tucker, D. M. Baney, W. V. Sorin, and C. A. Flory, "Thermal noise and radiation pressure in MEMS Fabry-Perot tunable filters and lasers," *IEEE J. Sel. Topics Quantum Electron.*, vol. 8, no. 1, pp. 88–97, Jan./Feb. 2002.



Nicolas Pavy received the Master's degree in micro- and nanotechnology from the Université Sciences et Technologies de Lille, Lille, France, in 2005. His thesis topic was the study of coplanar waveguides on ferroelectric materials.

In 2006, he joined Auxitrol, Esterline Sensor Group, where he worked on pressure sensors for aeronautics. Since 2008, he has been with ESIEE, Université Paris-Est, Noisy-le-Grand, France, as a clean-room process engineer. His interests include optical MEMS, inertial, and fluidic sensors.



Yves-Alain Peter (S'93-M'03-SM'07) received the M.Sc. degree in physics and the Dr. Sc. degree in sciences from the University of Neuchâtel, Neuchâtel, Switzerland, in 1994 and 2001, respectively.

In 1995, he was a Research Associate in the Medical Radiobiology Department, Paul Scherrer Institute, Switzerland. During 1995–2001, he was a Graduate Research Assistant with the Applied Optics Group, Institute of Microtechnology, University of Neuchâtel. From 2001 to 2003, he was a Postdoctoral Researcher with the Microphotonics Group, Stanford University, Stanford, CA. From 2003 to 2004, he was an R&D Engineer and the Project Leader with the Swiss Center for Electronics and Microtechnology, Switzerland. He is currently an Associate Professor in the Department of Engineering Physics, Ecole Polytechnique de Montréal, Montréal, QC, Canada. His research interests include microoptoelectromechanical systems and tunable nanophotonics structures.



Ai-Qun Liu (M'03) received the Ph.D. degree from the National University of Singapore, Singapore, in 1994, the M.Sc. degree from Beijing University of Posts and Telecommunications, Beijing, China, in 1988, and the B.Eng. degree from Xi'an Jiaotong University, Xi'an, China, in 1982.

Currently, he is a Professor in the Division of Microelectronics, School of Electrical and Electronic Engineering, Nanyang Technological University, Singapore. He serves as an editor, co-editor, and editorial board member of more than ten scientific journals. He is the author or coauthor of over 200 publications including peer-reviewed journal papers. He authored two books entitled *Photonic MEMS Devices—Design, Fabrication and Control* and *RF MEMS Switches and Integrated Switching Circuits*.

Prof. Liu won the IES Award in 2006 and the University Scholar Award in 2007.



Tarik Bourouina (A'00-M'02-SM'05) was born in 1967. He received the M.Sc. degree in physics from the University Houari Boumediene, Algeria, in 1987, the *Diplôme d'Etudes Approfondies* in electronics from the University of Paris-Sud Orsay, Orsay, France, in 1988, the Doctorat (Ph.D. degree) from the University of Paris XII Creteil, Creteil, France, in 1991, and the *Habilitation à Diriger les Recherches* degree from the University of Paris-Sud Orsay in 2000.

He started research in MEMS at the ESIEE Engineering School of Paris in 1988, where he conducted projects in the field of silicon-based acoustic microsensors, including microphones and the acoustic microgyroscope. In 1995, he joined the Université Paris-Sud-Orsay in the Institut d'Electronique Fondamentale, a joint laboratory with the Centre National de la Recherche Scientifique. From 1998 to 2001, he was with The University of Tokyo, Japan, as an invited scientist in the framework of the Laboratory of Integrated Micro Mechatronic Systems. He is currently a Professor at ESIEE, Université Paris-Est, Noisy-le-Grand, France. His research interests include microsensors, microanalysis systems, and optical MEMS.



Maurine Malak (S'07) was born in Cairo, Egypt, in 1983. She received the B.Sc. degree in electronics and communication engineering (ECE) and the M.Sc. degree in integrated optics from Ain Shams University (ASU), Cairo, in 2004 and 2008, respectively. Her M.Sc. thesis focused on the design of photonic devices for CWDM systems. She is currently working toward the Ph.D. degree in optical MEMS at ESIEE, Université Paris-Est, Noisy-le-Grand, France.

From 2004 to 2008, she was with the Optical Communication and Laser laboratory of ECE, ASU, as a Research Assistant. Her current research interests include research and design of optical MEMS components for vibration sensing and optical spectroscopy.



Frédéric Marty was born in 1971. He received the ESTE degree in microelectronics from ESIEE, Paris, France, and the M.S. degree in electronics from ISEN, Lille, France.

He worked for six years at various companies involved in MEMS and manufacturing, particularly in the field of pressure measurement and acceleration for aerospace and automotive applications. Since 1998, he has been with the ESIEE Engineering School of Paris, where he is engaged in microsystems developments and is in charge of various industrial projects, from design to fabrication in clean-room conditions. His current research interests include development of new prototypes of fluidic and pressure MEMS.

His current research interests include development of new prototypes of fluidic and pressure MEMS.